Front. Chem. China 2011, 6(3): 164–172
DOI 10.1007/s11458-011-0250-9

REVIEW ARTICLE

Mechanism and kinetics for methanol synthesis from CO_2/H_2 over Cu and Cu/oxide surfaces: Recent investigations by first-principles-based simulation

Qiuyang SUN and Zhipan LIU (✉)

The efficient fixation and utilization of CO_2 has been consistently pursued by chemists for decades. Although Cu-based catalysts, e.g., $Cu/ZnO/Al_2O_3$, have been widely used in industry for methanol synthesis from CO_2 hydrogenation ($CO_2 + 3H_2 \rightarrow H_3COH + H_2O$), many issues on the mechanism and the kinetics remain largely uncertain. For example, the surface site for CO_2 activation and the synergetic effect between Cu and oxide have been hotly debated in literature. In the past few years, theoretical modeling on pure Cu surfaces and Cu/oxide interfaces has been utilized to provide insight into these important questions. Here we will review the recent theoretical advances on simulating this complex heterogeneous catalytic process with first principles density functional theory (DFT) calculations and kinetics modeling. The theoretical results on the mechanism and the kinetics are compared and summarized.

Keywords density functional theory calculation, CO_2 hydrogenation, methanol synthesis, Cu-based catalysts, review

1 Introduction

The chemical conversion of CO_2 is of great interest nowadays because it not only removes greenhouse gas but also yields useful fuels and chemicals such as methanol. As one of the most promising route, methanol production by the hydrogenation of CO_2 has been extensively studied in experiment and it was found that this reaction can be catalyzed by metal and metal oxide composites such as Cu supported on ZrO_2, ZnO, etc. Cu/ZnO is a major type catalyst widely used in industry [1–3], which is often further modified by other addictives such as Al_2O_3 [4–6], ZrO_2 [4,7], Ga_2O_3, Cr_2O_3 [4], and metals such as Pd [5]. ZrO_2-supported Cu catalyst also attracted some attention for its good thermal stability as well as the high activity and selectivity [8–12]. Experimental studies on CO_2 hydrogenation over Cu model catalyst surfaces can be dated back to 1980s, in which the active surface structure and the reaction intermediates have been probed via various surface science techniques. For example, Campbell and coworkers demonstrated that pure Cu can already act as a catalyst for methanol synthesis and found that CO is the major product at the low conversion limit [13,14]. One of the major challenges for CO_2 hydrogenation is to control the selectivity to avoid the production of unwanted CO, which is believed to be formed through the reverse water gas shift (RWGS, $CO_2 + H_2 \rightarrow CO + H_2O$). A possible solution, for example, is to further convert methanol to methanol formate ($HCOOCH_3$) by shifting the reaction equilibrium toward methanol related product, as demonstrated recently for CO_2/H_2 over Cu/ZnO catalyst in the solvent of methanol [6,7].

Owing to the fact that Cu itself is capable to catalyze methanol synthesis, the catalytic role of the metal oxide becomes largely unclear. Burch et al. has revealed a paradoxical phenomenon that by adding ZnO (to Cu), the specific activity is shown to be improved by one order of magnitude while the activity can be correlated well with the copper surface area rather than ZnO content [15]. It was also found that the selectivity to methanol varies significantly from catalyst to catalyst and is also sensitive to reaction condition, e.g., from $< 1\%$ [3,13] to $> 99\%$ [4]. To understand these puzzles, experimental studies on model catalysts using various techniques, especially in situ infrared spectrum [16], have been carried out to shed light into the microscopic mechanism of the reaction. It was shown that HCOO and H_3CO are present as the common intermediates on different catalysts, implying that the addition of oxides, however, may not change markedly the catalytic mechanism. On the other hand, theoretical simulations, in particular those based on first principles calculations, have demonstrated their ability in providing deep insight into the microscopic mechanism and the kinetics of heterogeneous catalytic process including those at the solid-gas interface and solid-liquid interface [17–22]. Recent years have witnessed the great progress in theoretical simulations to resolve the atomic level picture on the reaction mechanism and kinetics of methanol synthesis from CO_2 hydrogenation [3,23–32].

Received August 22, 2011; accepted August 25, 2011
Shanghai Key Laboratory of Molecular Catalysis and Innovative Materials, Department of Chemistry, Key Laboratory of Computational Physical Science (Ministry of Education), Fudan University, Shanghai 200433, China
E-mail: zpliu@fudan.edu.cn

In this review, we aim to provide an overview of the current understandings on the mechanism and the kinetics of methanol synthesis from CO_2/H_2 based on recent DFT-based theoretical simulations. The theoretical models and computational tools involved will be introduced. The theoretical results obtained on different model catalysts will then be compared and summarized. We intend not only to highlight the consensus achieved, but also to discuss the remaining puzzles on some of the most important issues, including the active site for the activation of CO_2, and the synergetic effect between Cu and oxides.

2 Theoretical methods for modeling heterogeneous reactions

Of the many electronic structure techniques that have been developed, DFT based on Kohn-Sham equation is the most popular and robust theoretical approach currently available for solving the electronic structures of solid surfaces [33–36]. Pseudopotentials, such as Ultrasoft Vanderbilt pseudopotential [37] and Troullier–Martins norm-conserving pseudopotential [38] were widely utilized to describe valence electrons in solving Kohn-Sham equation. For solid surfaces, the exchange-correlation functionals utilized were generally at the level of local density approximation with the generalized gradient correction (GGA), such as PW91 [39] and Perdew–Burke–Ernzerf (PBE) [40]. A variety of basis sets can be chosen in DFT calculations, and in solid-state surface calculations the typical basis set is plane wave. Recent studies have suggested that carefully constructed numerical atomic orbitals can also be utilized to describe the surface properties of metals at the level of accuracy comparable to the plane-wave calculations [41]. Because of the huge saving in computational power in computing the electronic structure of large systems, the computational methods based on numerical atomic orbitals is particularly useful for simulating large metal/oxide composite systems as encountered in CO_2 hydrogenation.

The mainstream model to model surfaces is the periodic slab model. Conventional techniques utilized in the bulk calculations of solid, such as the Brillouin-zone k-point sampling techniques (e.g., Monkhorst–Pack scheme [42]), can be seamlessly transformed to study the surface properties with the periodic slab approach. For example, it was reported that Cu(111) [3,27] and m-$ZrO_2(\bar{2}\,12)$ [23,28] surfaces are modeled by three-layer slabs with a vacuum thickness more than 10 Å, where a part of [3,23,28] or all [27] the substrate atoms are fixed in their bulk truncated positions. A large unit cell is often essential in the modeling of reactions on surfaces in order to minimize the interaction between adsorbates across repeated unit cells. This is also required in simulating the interface between different materials where a good lattice match is needed.

An efficient way to locate the transition state (TS) of reactions is highly desirable in computational simulation since the reactivity depends critically on the barrier height (E_a), the energy difference between the TS and the initial state (IS). Due to the lack of analytic Hessian in calculations with non-Gaussian basis sets, the traditional TS-searching methods by eigenvalue following is not a practical approach in periodic slab calculations. Instead, the first-derivative-based methods are widely utilized for locating the TS of surface reactions, which are in general highly demanding in computational power. The typical methods utilized include nudged-elastic-band (NEB) method [43], the bond constrained methods [44], dimer-based method [45,46], and synchronous transit methods [47]. Rcently, Liu and coworkers developed the Constrained–Broyden–Minimization method [44] and Constrained–Broyden-dimer methods [46], which are found to be efficient for finding the TS of complex reactions on surface.

First-principles based kinetics simulations, such as microkinetic method and kinetic Monte Carlo (kMC) method, have been utilized in recent years to predict the reaction rates and the selectivity of complex surface reactions. These kinetics simulations can deal with complex systems on time scales of the order of seconds or even longer, which cannot be achieved by typical molecular dynamics simulations. In reality, it is the free energy of reactions that determines the reaction kinetics, and thus the calculated DFT total energy must be amended by the necessary zero-point correction and entropy terms to derive the free energy, which can either be calculated from first principles or obtained from standard thermodynamics data in experiment. The use of a mean-field microkinetic model requires that the adsorbates on the surface be well-mixed and diffusion limitations be negligible. The situations should therefore be taken with caution when the reaction occurs only on a minority of surface sites or the diffusion barrier is high for some key species. On the other hand, kMC simulations are capable of accounting for the correct local structure and coverage [48], and are yet much more costly if performed properly. Recently, kMC simulation based on the Bortz–Kalos–Lebowitz algorithm [49,50] was utilized by Liu and coworkers for the study of the CO_2 hydrogenation at the Cu/ZrO_2 interface [28]. It should be emphasized that the lateral adsorbate-adsorbate interactions may strongly influence the stability of intermediates, and thus the coverage-dependence of the kinetics parameters should be considered properly in kinetics simulation. The intrinsic inaccuracy of the current DFT functionals in dealing with the adsorption/desorption energetics should also be paid attention in kinetics simulations [23], although the energy

difference between states on surfaces are believed to be more accurate.

3 Surface models and general consensus

To reveal the mechanism and kinetics of methanol synthesis from CO_2 hydrogenations, various theoretical models have been utilized, ranging from small Cu clusters to extended Cu surfaces and to Cu/ZrO_2 interfaces, as illustrated in Fig. 1. Before we elaborate on more detailed result of each surface model, it is worth outlining first the general consensus achieved from these theoretical investigations.

It was generally accepted that in CO_2 hydrogenation the adsorbed atomic H are present, which comes from the dissociation of H_2. This is because H_2 can readily dissociate to H atoms on Cu surfaces at reaction temperatures (e.g., 500 K). The dissociative adsorption energy is around 0.3 eV per H_2 molecule [3,27] from various DFT calculations. On the other hand, whether CO_2 can adsorb strongly on the catalyst surface is a major question. It is found that on the neutral Cu models including Cu nanoparticles, CO_2 can only weakly physisorb with very low binding energy (< 0.1 eV [3,27]). The hydrogenation of CO_2 on pure Cu surfaces is therefore most likely via the Eley-Rideal (ER) mechanism, where the gaseous CO_2 is directly hydrogenated by the adsorbed H atom. In the presence of oxide supports, as CO_2 can adsorb at the Cu/oxide interface (e.g., 0.69 eV on ZrO_2 [23]), it becomes possible that CO_2 hydrogenation occur via the Langmuir–Hinshelwood (LH) mechanism. The alternative pathway via CO_2 decomposition can also not be ruled out, especially in Cu/oxide composite systems.

In Table 1, we summarize the reported key surface species of CO_2 hydrogenation, together with the rate determining steps and their barriers, E_a. From Table 1, it can be seen that three reaction intermediates are shared in different studies, namely HCOO, H_2CO and H_3CO, in consistent with the experimental findings. For the transformation of HCOO to H_2CO, two likely pathways have been reported, either via HCOOH and H_2COOH, or via H_2COO. Although the reported rate determining step differs sharply between different studies, it is in general that CO_2 hydrogenation is highly activated with the calculated reaction barriers being larger than 1 eV.

4 Mechanism from different models

4.1 Cationic Cu

In the 1990s, Kakumoto et al. [24,25] carried out ab initio calculations to study the stability of the reaction intermediates in methanol synthesis by CO_2 over small Cu, CuO and CuZnO clusters [24]. While the models are too simplified compared to real catalyst surfaces, some useful insights have been provided. They found that CO_2 and the following intermediates can adsorb on Cu^+ sites, while H_2 adsorbs on both metallic copper and ZnO to form H atoms and H^+/H^-,

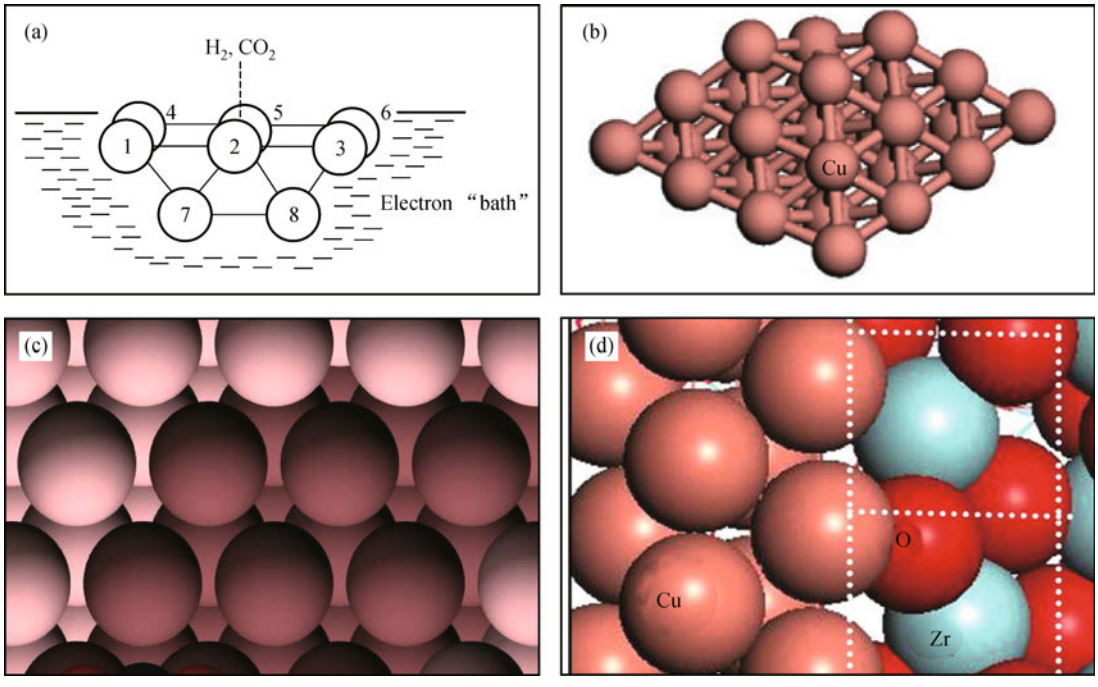

Figure 1 (a) A model adcluster for Cu(100); (b) a Cu_{29} nanoparticle; (c) Cu(111) surface; (d) Cu strip at the stepped m-$ZrO_2(\bar{2}\,12)$. Reprinted from Refs. [3,17,26,27] respectively.

Table 1 Mechanisms of methanol synthesis from CO_2/H_2 determined on different Cu-based model systems

Catalyst	C-containing intermediates	Rate determining step(s)	E_a/eV
Cu^+ [25]	$HCOO^-$,H_2CO, H_3CO^-	_	_
Cu(100) [26]	HCOO, H_2COO, H_2CO, H_3CO	HCOO* + H*→H_2COO	1.00
Cu(111) [27]	HCOO, HCOOH, H_2COOH,	H_3CO* + H*→H_3COH*;	1.17;
	H_2CO, H_3CO	OH* + H*→H_2O*	1.18
Cu(111) [3]	HCOO, H_2COO	H_2COO* + H*→H_2CO* + OH*	1.60
	H_2CO, H_3CO		
Cu_{29} [3]	HCOO, H_2COO	H_2COO* + H*→H_2CO* + OH*	1.41
	H_2CO, H_3CO		
Cu/ZrO_2 [23]	HCOO, H_2COO, H_2COOH,	H_2COO* + H*→H_2COOH*;	1.30;
	H_2CO, H_3CO	H_3CO* + H*→H_3COH*	1.28

respectively. The important intermediates for the methanol synthesis were bridging-formate, formaldehyde, and methoxy. The reaction route can be summarized as: CO_2→CO_2*→$HCOO^-$*→H_2CO*→H_3CO^-*→H_3COH (hereafter * denotes an adsorbed state). From thermodynamics, the most endothermic step is the formaldehyde hydrogenation to methoxy (+ 0.46eV), and this route appears to proceed facilely. It was noticed that the stability of some adsorbates and the reaction barrier of key reactions can be changed by changing the electronic state of the model clusters [25]. For example, the stability of formate and formaldehyde intermediates increases as the total charge increases, while the stability of methoxy species was almost constant for the total charge from 0 to + 0.4. The total atomic charge distributions on Cu/CuO and Cu/ZnO clusters showed that the cationic copper locate only on the boundary of Cu and the oxide. It is expected that the increase of the interfacial Cu by finely dispersing Cu on oxides can help to increase the number of active sites.

4.2 Cu single crystal surfaces

In 1999, Nakatsuji and coworkers [26] studied the mechanism of the hydrogenation of CO_2 to methanol on a Cu(100) surface using the dipped adcluster model (DAM) combined with ab initio Hartree–Fock (HF) and second-order Møller–Plesset (MP2) calculations. A Cu_8(6,2) cluster, which contains six copper atoms in the first layer and two copper atoms in the second layer was used to model the Cu(100) surface (Fig. 1a). The dipped adcluster model [45] was used to include the effects of the bulk metal, such as electron transfer between the admolecule and the surface, and the image force. Based on this Cu cluster model, they evaluated the possible reaction pathway with the LH mechanism starting from the coadsorption of H_2 and CO_2 state. In the DAM of Cu(100), the chemisorbed CO_2 exists as a bent anionic CO_2^- species, with both O atoms bonding with surface copper. About one electron is transferred from the metal surface to the π* orbital of CO_2, making the CO_2 very reactive. (This is however not confirmed later by DFT-slab calculations). Five successive hydrogenations occur later in the hydrogenation of adsorbed CO_2 to methanol involving formate, dioxomethylene, formaldehyde and methoxy: CO_2*→HCOO*→H_2COO*→H_2CO*→H_3CO*→H_3COH. Among the hydrogenation steps, the hydrogenation of adsorbed formate to adsorbed dioxomethylene is the highest barrier elementary step (HCOO* + H*→H_2COO*; E_a = 1.00 eV; ΔE = 0.74 eV). Another high barrier reaction calculated is the hydrogenation of adsorbed dioxomethylene to yield formaldehyde (H_2COO* + H*→H_2CO* + OH*; E_a = 0.74 eV). The authors suggest that the high energy barrier associated with the unstable dioxomethylene intermediate may account for the lower activity of a clean copper surface compared to the copper-based catalyst in practical methanol synthesis.

Grabow and Mavrikakis [27] recently reported the mechanism of methanol synthesis through CO_2 and CO hydrogenation on Cu(111) using DFT and microkinetics modeling. Some unusual reaction intermediates such as formic acid (HCOOH) and hydroxyl-methoxy (CH_3O_2) were taken into account in the reaction pathway, which allows for the formation of formic acid (HCOOH), formaldehyde (CH_2O), and methyl formate ($HCOOCH_3$) as by-products. The mean-field microkinetics model was utilized to predict the reaction kinetics, where all kinetic parameters were initially taken from DFT calculations and subsequently fitted to the experimental rate data. It is noticed that the experimental kinetic data are collected in a spinning basket reactor at pressures 15–50 atm and temperatures 483–547 K over a $Cu/ZnO/Al_2O_3$ catalyst with various $H_2/CO_2/CO$ feed compositions, which is not exactly Cu(111) surface. Theoretically, a CSTR model was employed to simulate the spinning basket reactor; the number of Cu sites used is 300 μmol(sites)/g(catalyst). Because the DFT data are from (111) surface while the experiment was performed on metal/oxide composite catalyst, the authors therefore adjusted the DFT-based kinetic parameters such as the enthalpy of species and the proximity factors of the TS in order to reproduce the

experimental kinetic data. By comparing the DFT data with the fitted data, they found that generally the species are better stabilized on the catalyst surface than on Cu(111) from DFT. The deviation is rather large, being 0.3–0.6 eV for most intermediates such as OH*, COOH*, HCO*, HCOO*, HCOOH*, CH_3O_2*, H_2CO*, H_3CO*, and H_3COH*, except for H* and CO* where the deviation is ~0.1 eV.

Both CO and CO_2 hydrogenation pathways are found to be active for methanol synthesis under typical methanol synthesis conditions. The CO_2 pathway for methanol synthesis starts from the formation of formate (HCOO*) from CO_2* and H* on Cu(111) surface, and the following intermediates include HCOOH*, CH_3O_2*, CH_2O*, and CH_3O*. Besides the CO_2 pathway, the hydrogenation of CO can also yield methanol through the pathway: CO* → HCO* → CH_2O* → H_3CO* → H_3COH*. The potential energy surface of the major CO_2 hydrogenation pathway is given in Fig. 2. This reaction mechanism differs from the one on Cu(100) by Nakatsuji and coworkers [26] in three aspects. First, the obvious electron transfer that assists the chemsorption of CO_2 [26] is not observed in the DFT-slab calculation. CO_2 only physisorb on Cu(111) surface with a weak binding energy of 0.08 eV. Second, the hydrogenation of HCOO* leads to HCOOH* instead of dioxymethylene (H_2CO_2*). Third, the hydroxyl-methoxy (H_2COH, CH_3O_2) intermediate is present in two elementary reactions, namely, HCOOH* + H*→ CH_3O_2* and CH_3O_2*→CH_2O* + OH*. The CH_3O_2 is not studied in the work by Nakatsuji and coworkers [26].

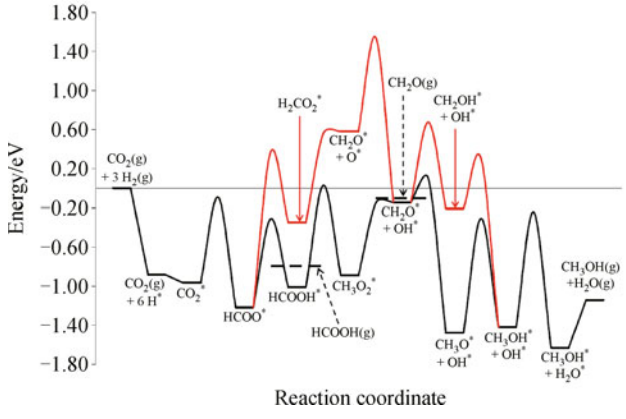

Figure 2 Potential Energy Surface (PES) of methanol synthesis on Cu (111) from CO_2 through competing pathways. The black line indicates the lowest energy pathway through the: HCOO*, HCOOH*, CH_3O_2*, CH_2O* and CH_3O* intermediates. The main intermediates along the red path are: HCOO*, H_2CO_2*, CH_2O*, and CH_2OH*. The two dashed horizontal lines indicate the desorption barriers of HCOOH and CH_2O. Reprinted from Ref. [27].

The reaction kinetics such as the rate-limiting steps and the contributions of each pathway is analyzed based on the microkinetic simulation. The hydrogenation of H_3CO* is slow, the rate of which qualitatively describes the behavior of overall methanol synthesis rates for a large range of conditions and CO_2-rich feed compositions. However, under some conditions, especially for CO-rich feeds, the formation of CH_3O* (CH_2O* + H*→CH_3O*) can be rate limiting, resulting in a volcano shaped curve for methanol production as a function of the $CO_2/(CO + CO_2)$ feed ratio. The relative contributions of CO and CO_2 hydrogenation pathways are determined by their corresponding slow steps, namely, HCO* + H* → CH_2O* + * in the CO route and HCOOH* + $H^* \rightarrow CH_3O_2^* + *$ in the CO_2 route, and also by the feed composition and reaction conditions. Under typical industrial conditions (t = 499.3 K, P = 29.9 atm, molar fractions of CO, CO_2 and H_2 in the feeding gas are 0.053, 0.047, 0.90, respectively), it is found that 2/3 of methanol is produced from CO_2 hydrogenation.

By comparing the binding energies calculated with DFT on the Cu(111) surface and the parameters obtained from fitting, Grabow and Mavrikakis suggested that the merely clean Cu(111) surface cannot provide an accurate representation of the active site on a commercial $Cu/ZnO/Al_2O_3$ catalyst. Instead, more open and partially oxidized Cu facet, such as Cu(110), Cu(100), Cu(211), might be a more suitable representation of the active site for methanol synthesis. Although it seems likely that only the Cu particles are responsible for the catalytic activity of the real catalyst, the synergistic effects involving the oxide support such as ZnO cannot be excluded. The fitted kinetics model also depends heavily on the experimental data, which are taken mainly from the CO_2-rich conditions. The discrepancies also exist between the theoretical predictions and the data from CO-rich feed compositions in experiment. It might be caused by an adsorbate (CO)-induced surface reconstruction during a shift from oxidizing (CO_2-rich) to reducing (CO-rich) conditions, which, in turn, could affect the dominant reaction mechanism. For more quantitative conclusions about the structure sensitivity of the reaction and the oxidation state of the surface, further studies are needed.

4.3 Cu nanoparticles

Yang et al. [3] utilized a Cu_{29} nanoparticle as the model catalyst to investigate mechanol synthesis from CO_2 hydrogenation. The Cu_{29} nanoparticle has a pyramidal shape exposing only (100) and (111) facets with a diameter of 1.2 nm (Fig. 1b). Experimentally, they also showed that the clean O-terminated ZnO(000$\bar{1}$) surface was inactive as a catalyst [11], and therefore it is important to examine the activity of pure Cu nanoparticles, in which the low-coordinated sites and the shape flexibility of the nanoparticle

may play key roles in the catalytic process.

It was found that H_2 can dissociate on Cu_{29} spontaneously as H–H bond breaks during the geometry optimization. After H_2 dissociation, the atomic hydrogen binds to the top sites of Cu_{29} with a binding energy of −0.34 eV. In the presence of adsorbed H atoms, CO_2 molecule cannot bind to the nanoparticle. This is consistent with the experimental observation that the increase of adsorbed H coverage hinders only the dissociative adsorption of H_2 on Cu, but not the adsorption of CO_2 [52].

The CO_2 activation is initiated via an Eley-Rideal (ER) mechanism, in which the gaseous CO_2 directly reacts with an adsorbed H atom to form HCOO. The formate pathway occurs via intermediates H_2COO, H_2CO and H_3CO, and the rate-limiting step is the H-assisted H_2COO dissociation, i.e., $H_2COO + H \rightarrow H_2CO + OH$ (E_a = 1.41 eV, ΔE = 0.45 eV). The results on Cu_{29} nanoparticle are similar to those provided by Mavrikakis et al. [20] on Cu(111) surface except that (i) H_2COO is thermodynamically preferred to HCOOH as an intermediate by 0.82 eV on the nanoparticle, and (ii) H_2COOH may not be present on the nanoparticle since the reaction barrier to form H_2COOH is 1.69 eV, higher than that of H-assisted dissociation of H_2COO (1.41 eV).

Yang et al. [3] also considered the competing RWGS reaction on the Cu_{29} nanoparticle. In this mechanism, CO_2 is first hydrogenated to HOCO, which splits later to CO and OH. The OH is finally converted to water. The barrier of the rate limiting step of the RWGS ($H^* + OH^* \rightarrow H_2O^*$) is 0.27 eV lower than that of methanol synthesis (1.14 eV vs. 1.41 eV). This suggests that at t = 573 K RWGS reaction is 2–3 orders of magnitude faster, and that the dominant product on Cu catalyst is CO rather than methanol. The calculations also indicate that CO produced by the fast RWGS reaction does not undergo subsequent hydrogenation to methanol, but instead, simply accumulates as a product. The possible methanol production from CO hydrogenation may be via the intermediates HCO, H_2CO, H_3CO, but this pathway is hindered by the hydrogenation of CO to HCO. HCO is not stable and tends to dissociate back to CO and H atoms on Cu with a barrier of only 0.03 eV. Therefore, Yang et al. [3] suggested that methanol selectivity over Cu-based catalysts can be improved by adding dopants/promoters that are able to stabilize HCO species or facilitate the hydrogenation of HCOO and H_2COO.

They also performed calculations of the same reaction pathways on Cu(111) surface [3], and found the Cu nanoparticle model shows a higher activity (see Fig. 3). Compared with that on Cu(111), the barrier for the rate-limiting step of methanol synthesis reaction on Cu_{29} is 0.19 eV lower (1.41 eV compared with 1.60 eV), which corresponds to a reaction rate of ~50 times faster (t = 573 K). They suggested that the higher activity of the nanoparticle is associated with its large stabilization effect on the key intermediates, e.g., formate and dioxomethylene. The theoretical results illustrate that the particle size of Cu catalyst could be important in methanol synthesis.

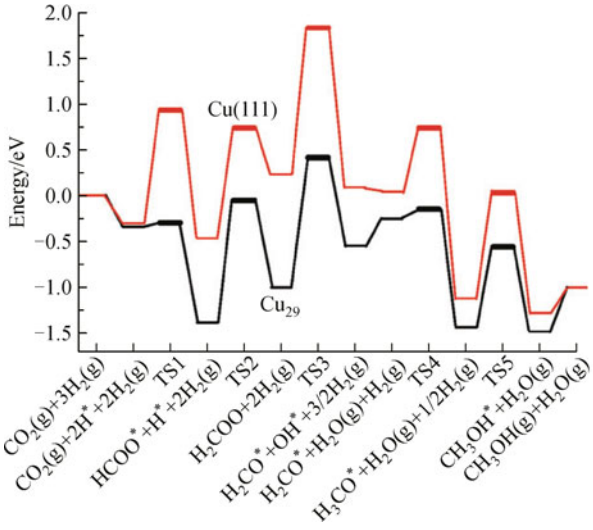

Figure 3 Potential energy diagram for the methanol synthesis reaction on the Cu(111) surface and Cu_{29} nanoparticle, where the thin bar represents the intermediates and the thick bar represents the transition states. The upper diagram corresponds to Cu(111) and the lower diagram corresponds to Cu_{29}. Reprinted from Ref. [3]

4.4 Cu/ZrO_2 interface

In the series works of Liu and coworkers [23,28,29], the catalytic kinetics of CO_2 fixation to methanol over a binary catalyst Cu/ZrO_2 have been investigated by first principles kinetic Monte Carlo simulation. Instead of the clean Cu models described above, they established a Cu/ZrO_2 interface model and explored the reaction network of CO_2 hydrogenation. In establishing the binary catalyst model, they first screened the possible active surface facetsof ZrO_2 support. It was reported that metal cationic monomers and metal particles anchor preferentially at oxide defected sites. The binding energies of a Cu adatom at $ZrO_2(\bar{1}\,11)$ and $ZrO_2(\bar{2}\,12)$ are 0.99 and 1.08 eV, less than one third of the calculated cohesive energy of bulk Cu, 3.55 eV. The growth of metallic Cu particles over the oxide surfaces is thus preferred thermodynamically. Furthermore, the DFT calculations for CO_2 adsorption on bare ZrO_2 also showed that CO_2 adsorbs more strongly at the stepped $ZrO_2(\bar{2}\,12)$ than at the flat $ZrO_2(\bar{1}\,11)$ (1.58 eV compared with 0.83 eV), which implies that the defected ZrO_2 is chemically more active in activating CO_2. To represent the atomistic structure of the Cu/ZrO_2 interface, a two-layer close-packed Cu strip was added onto $ZrO_2(\bar{2}\,12)$ stepped surface because the stepped oxide can provide a better geometry for both the adsorption of the Cu strip and the

reactant CO_2. This interface structure exposes only the most stable facets of the two components, i.e., the ($\bar{1}$ 11) terrace of ZrO_2 and (111)-like Cu surface. Two kinds of Zr, the five-coordinated (Zr5c) and six-coordinated (Zr6c) lattice Zr are exposed, which are separated by oxygen atoms at the interface (Fig. 1d).

The adsorption of reactants on the interface was reported. CO_2 adsorbs preferentially on the ZrO_2 sites of the Cu/ZrO_2 interface [21]. The calculated Ead of CO_2 is 0.69 eV. The best configuration of CO_2 adsorption features a tri-dented anchoring geometry: its two O and C atoms bond with the Zr_{6c}, Zr_{5c} and O_{2c}, respectively. The strong chemisorption of CO_2 is not observed in pure Cu models, which is an important advantage of the Cu/oxide interface as the fixation and activation of CO_2 can now follow the LH mechanism. H atoms adsorb strongly only on the Cu sites. The H atom adsorption energy at the Cu strip is 2.64 eV with respect to the gas phase H atom, which is much stronger than the H adatoms at the ZrO_2 side (1.76 eV) by forming OH with interface O_{2c}. Kinetically, H_2 dissociation on Cu only requires a reaction barrier of 0.38 eV on the Cu strip, which is consistent with the general consensus that H_2 adsorbs dissociatively on Cu [53]. Obvioiusly, CO_2 hydrogenation can occur at the interface starting from CO_2 at the ZrO_2 and H on the Cu. Two routes leading to methanol, namely, the formate route and the RWGS route (featuring the splitting of CO_2 in the production of CO and atomic O at the interface) as suggested by experiments [54–56], were both identified.

In the RWGS route, the adsorbed CO_2 dissociates directly at the interface, forming the adsorbed CO and atomic O. By stepwise hydrogenation to formyl (HCO) and formaldehyde (H_2CO), CO is converted to methylate (H_3CO). H_3CO can be further hydrogenated to methanol (H_3COH). Meanwhile, the surface atomic O can react with H to form hydroxyl and water. In parallel with the RWGS pathway, the adsorbed CO_2 can alternatively react with H to yield the surface formate (HCOO). Upon further hydrogenation, HCOO is converted to H_2COO and H_2COOH. The interfacial H_2COOH can dissociate to formaldehyde (H_2CO) and hydroxyl (OH), which can be further hydrogenated to methanol and water, respectively. The HCOO and H_2COO are the most stable intermediates, while H_2COOH and H_2CO are the least stable surface species.

Based on the kinetic Monte Carlo simulation on this model, Liu and coworkers [28] found that the interface sites are largely occupied by oxidative species, such as O atoms, OH and H_3CO groups and, therefore, the interface Cu atoms are cationic. This means that the appearance of cationic Cu is just a natural consequence of the catalytic process. The in situ formation of cationic Cu seen from kMC simulation may help rationalize the experimental observations, where the ionic copper was identified during methanol synthesis from CO_2/H_2. To describe more realistically the interfacial Cu, in the later work [23], Hong and Liu adopted an oxygen-rich interface as the new model to mimic the catalyst under experimental conditions, where the exposed Zr_{5c} sites are already blocked by the oxygen species. With a switch to the Zr_{6c} model, the adsorption energies of oxygen-containing species like O and H_3CO are indeed much reduced, which effectively prevents the poisoning of the model catalyst in the kinetics simulation.

In the oxygen-rich interface model, both microkinetics and the kMC [23] simulation were carried out. The temperature, total pressure and molar ratio of CO_2 to H_2 were set at 500 K, 17 atm and 1∶3 respectively. The equilibrium simulation shows that CO_2 conversions to H_3COH and CO are 12.5% and 6.2%, respectively. From the dynamic simulation based on the continuous stirred tank reactor model, the following results are obtained. (i) 90% of the converted CO_2 molecules are hydrogenated to formate, while only a few of them are decomposed to CO. Both methanol and CO are produced dominantly via the formate pathway (see Fig. 4) through the direct hydrogenation of CO_2. The dissociation of CO_2 is the slowest step. H_2CO is a key intermediate species in the reaction pathway, the hydrogenation of which dictates the high temperature of CO_2 hydrogenation. (ii) Formate, H_2COO and CO are formed instantaneously as the reaction starts and their concentrations hardly change during the reaction. On the contrary, H_3CO is low in concentration at the beginning, but its coverage continuously increases at the first ten minutes of the reaction. (iii) The conversion of CO_2 is 1.2% with the selectivity to H_3COH being 68%. The TOF is calculated to be 2.4×10^{-3} s^{-1}. (iv) The calculated apparent activation energies for CO and methanol formation are 1.79 and 0.79 eV, respectively, explaining why the selectivity to methanol

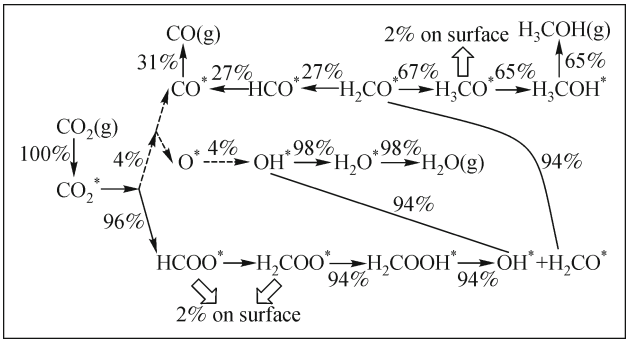

Figure 4 Proposed reaction mechanism of CO_2 hydrogenation over Cu/ZrO_2 according to kMC simulation results. Solid and broken lines are the major and minor routes, respectively. The percentage labeled on the arrows show contributions of elementary steps. Reprinted from Ref. [23]

decreases dramatically as the temperature increases. (v) The secondary reactions due to the readsorption of products lower the overall TOF but increase the selectivity to methanol by 16%.

Hong and Liu also compared the kMC simulation results with the microkinetics results [17]. It was found that the overall rate from microkinetics simulation is by and large overestimated compared to that from kMC simulation. As a mean-field approach, the rate expression in microkinetics assumes that the reactants have been mixed completely before they react with each other. Although this assumption may work well for the reaction in the gas phase or in solution, it is often not valid for heterogeneous catalytic reactions, where the active sites (e.g., the interface of composite) are in minority and the diffusion of reactants is kinetically hindered (e.g., a corrugated potential energy surface or local high surface coverage).

5 Concluding remarks

In this work, we review the recent theoretical advances of methanol synthesis from CO_2/H_2 over Cu-based catalysts. We summarize the typical theoretical approaches utilized in simulating the complex heterogeneous catalytic reactions. The CO_2 hydrogenation mechanism and kinetics from different model surfaces have been compared and analyzed. We show that this topic is not free from controversies despite many years' studies,in experiment and theory. This is not least because of the intrinsic complexity of the system, i.e., involving multi-reaction-channels and composite materials. The catalytic role of the charged Cu sites, nanosized Cu particle and the Cu/oxide interface have been highlighted in recent theoretical studies. The direct CO_2 hydrogenation is found to be a major reaction channel for methanol synthesis, while the CO hydrogenation pathway has only a minor contribution.

Due to the limitation of the computational power for direct simulating the complex metal/oxide composite systems, it remains difficult for computational simulation to address fully the "synergic effect" at the atomistic scale and reproduce the experimental kinetics at the real time scale. Although many early works agree that Cu is the only active catalytic component, recent results on Cu/oxide models suggest an alternative picture where the Cu/oxide interface play an important role in activating CO_2. Obviously, more work is needed in the near future to characterize the atomistic structure of the Cu/oxide interface and identify the reaction mechanism toward the rational design of better catalysts for methanol synthesis from CO_2 hydrogenation.

Acknowledgements This work was supported by the National Natural Science Foundation of China (No. 20825311), 973 program (No. 2011CB808500), Science and Technology Commission of Shanghai Municipality (No. 08DZ2270500) and Program for Professor of Special Appointment (Eastern Scholar) at Shanghai Institute of Higher Learning.

References

1. Strunk, J.; Kahler, K.; Xia, X.; Muhler, M., *Surf. Sci*. **2009**, *603*, 1776–1783
2. Ostrovskii, V. E., *Catal. Today* **2002**, *77*, 141–160
3. Yang, Y.; Evans, J.; Rodriguez, J. A.; White, M. G.; Liu, P., *Phys. Chem. Chem. Phys*. **2010**, *12*, 9909–9917
4. Saito, M.; Takeuchi, M.; Fujitani, T.; Toyir, J.; Luo, S.; Wu, J.; Mabuse, H.; Ushikoshi, K.; Mori, K.; Watanabe, T., *Appl. Organomet. Chem*. **2000**, *14*, 763–772
5. Yu, K. M. K.; Yeung, C. M. Y.; Tsang, S. C., *J. Am. Chem. Soc*. **2007**, *129*, 6360–6361
6. Yu, K. M. K.; Tsang, S. C., *Catal. Lett*. **2011**, *141*, 259–265
7. Lim, H. W.; Park, M. J.; Kang, S. H.; Chae, H. J.; Bae, J. W.; Jun, K. W., *Ind. Eng. Chem. Res*. **2009**, *48*, 10448–10455
8. J. Weigel, A. Koeppel, A. Baiker, A. Wokaun Langmuir 12 (1996) 5319.
9. Baker, J. E.; Burch, R.; Golunski, S. E., *Appl. Catal*. **1989**, *53*, 279–297
10. Koeppel, R. A.; Baiker, A.; Schild, C.; Wokaun, A., *Stud. Surf. Sci. Catal*. **1991**, *63*, 59–68
11. Shustorovich, E.; Bell, A. T., *Surf. Sci*. **1991**, *253*, 386–394
12. Sun, Y.; Sermon, P. A., *Catal. Lett*. **1994**, *29*, 361–369
13. Yoshihara, J.; Parker, S.; Schafer, A.; Campbell, C. T., *Catal. Lett*. **1995**, *31*, 313–324
14. Yoshihara, J.; Campbell, C. T., *J. Catal*. **1996**, *161*, 776–782
15. Burch, R.; Golunski, S. E.; Spencer, M. S., *Catal. Lett*. **1990**, *5*, 55–60
16. Wang, X.; Zhang, H.; Li, W.; Korean, J., *Chem. Eng*. **2010**, *27*, 1093
17. Liu, Z. P.; Wang, C. M.; Fan, K. N., *Angew. Chem. Int. Ed*. **2006**, *45*, 6865–6868
18. Wang, C. M.; Fan, K. N.; Liu, Z. P., *J. Am. Chem. Soc*. **2007**, *129*, 2642–2647
19. Chen, J.; Liu, Z. P., *J. Am. Chem. Soc*. **2008**, *130*, 7929–7937
20. Li, Y. F.; Liu, Z. P.; Liu, L.; Gao, W., *J. Am. Chem. Soc*. **2010**, *132*, 13008–13015
21. Shang, C.; Liu, Z. P., *J. Am. Chem. Soc*. **2011**, *133*, 9938–9947
22. Fang, Y. H.; Liu, Z. P., *J. Am. Chem. Soc*. **2010**, *132*, 18214–18222
23. Hong, Q. J.; Liu, Z. P., *Surf. Sci*. **2010**, *604*, 1869–1876
24. Kakumoto, T., *Energy Convers. Manage*. **1995**, *36*, 661–664
25. Kakumoto, T.; Watanabe, T., *Catal. Today* **1997**, *36*, 39–44
26. Hu, Z. M.; Takahashi, K.; Nakatsuji, H., *Surf. Sci*. **1999**, *442*, 90–106

27. L. C. Grabow, M. Mavrikakis, *ACS Catal*. 2011, 1, 365
28. Tang, Q. L.; Hong, Q. J.; Liu, Z. P., *J. Catal*. **2009**, *263*, 114–122
29. Tang, Q. L.; Liu, Z. P., *J. Phys. Chem. C* **2010**, *114*, 8423–8430
30. French, S. A.; Sokol, A. A.; Bromley, S. T.; Catlow, C. R. A.; Rogers, S. C.; King, F.; Sherwood, P., *Angew. Chem. Int. Ed*. **2001**, *40*, 4437
31. French, S. A.; Sokol, A. A.; Bromley, S. T.; Catlow, C. R. A.; Sherwood, P., *Top. Catal*. **2003**, *24*, 161–172
32. Catlow, C. R. A.; French, S. A.; Sokol, A. A.; Thomas, J. M., *Philos. Transact. A Math. Phys. Eng. Sci*. **2005**, *363*, 913–936, discussion 1035–1040
33. Payne, M. C.; Teter, M. P.; Allan, D. C.; Arias, T. A.; Joannopoulos, J. D., *Rev. Mod. Phys*. **1992**, *64*, 1045–1097
34. Kresse, G.; Hafner, J., *J. Phys. Condens. Matter* **1994**, *6*, 8245–8257
35. Soler, J. M.; Artacho, E.; Gale, J. D.; Garcia, A.; Junquera, J.; Ordejon, P.; Sanchez-Portal, D., *J. Phys. Condens. Matter* **2002**, *14*, 2745–2779
36. Junquera, J.; Paz, O.; Sanchez-Portal, D.; Artacho, E., *Phys. Rev. B* **2001**, *64*, 235111
37. Vanderbilt, D., *Phys. Rev. B* **1990**, *41*, 7892–7895
38. Troullier, N.; Martins, J. L., *Phys. Rev. B* **1991**, *43*, 1993–2006
39. Perdew, J. P.; Chevary, J. A.; Vosko, S. H.; Jackson, K. A.; Pederson, M. R.; Singh, D. J.; Fiolhais, C., *Phys. Rev. B* **1992**, *46*, 6671–6687
40. Perdew, J. P.; Burke, K.; Ernzerhof, M., *Phys. Rev. Lett*. **1996**, *77*, 3865–3868
41. García-Gil, S.; García, A.; Lorente, N.; Ordejón, P., *Phys. Rev. B* **2009**, *79*, 075441
42. Monkhorst, H. J.; Pack, J. D., *Phys. Rev. B* **1976**, *13*, 5188–5192
43. Henkelman, G.; Uberuaga, B. P.; Jonsson, H., *J. Chem. Phys*. **2000**, *113*, 9901
44. Wang, H. F.; Liu, Z. P., *J. Am. Chem. Soc*. **2008**, *130*, 10996–11004
45. Henkelman, G.; Jonsson, H., *J. Chem. Phys*. **1999**, *111*, 7010
46. Shang, C.; Liu, Z. P., *J. Chem. Theory Comput*. **2010**, *6*, 1136–1144
47. Halgren, T. A.; Lipscomb, W. N., *Chem. Phys. Lett*. **1977**, *49*, 225–232
48. Temel, B.; Meskine, H.; Reuter, K.; Scheffler, M.; Metiu, H. J., *Chem. Phys*. **2007**, *126*, 204711
49. Chatterjee, A.; Vlachos, D. G., *J. Comput. Aided Mater. Des*. **2007**, *14*, 253–308
50. Levi, A. C.; Kotrla, M., *J. Phys. Condens. Matter* **1997**, *9*, 299–344
51. Nakatsuji, H., *J. Chem. Phys*. **1987**, *87*, 4995
52. Nakano, H.; Nakamura, I.; Fujitani, T.; Nakamura, J., *J. Phys. Chem. B* **2001**, *105*, 1355–1365
53. Wambach, J.; Baiker, A.; Wokaun, A., *Phys. Chem. Chem. Phys*. **1999**, *1*, 5071–5080
54. Schilke, T. C.; Fisher, I. A.; Bell, A. T., *J. Catal*. **1999**, *184*, 144–156
55. Schild, C.; Wokaun, A.; Baiker, A., *J. Mol. Catal*. **1990**, *63*, 243–254
56. Jennings, J. R.; Lambert, R. M.; Nix, R. M.; Owend, G.; Parker, D. G., *Appl. Catal*. **1989**, *50*, 157–170